

ARTICLE



Arc weakens synapses by dispersing AMPA receptors from postsynaptic density via modulating PSD phase separation

Xudong Chen^{1,4}, Bowen Jia^{1,4}, Yoichi Araki², Bian Liu², Fei Ye¹, Richard Hugarir² and Mingjie Zhang^{1,3}✉

© CEMCS, CAS 2022

In response to stimuli, the immediate early gene product Arc can acutely down-regulate synaptic strength by removing AMPA receptors (AMPA) from synapses and thus regulate synaptic plasticity. How Arc, a scaffold protein, can specifically facilitate synaptic removal of AMPARs is unknown. We found that Arc directly antagonizes with PSD-95 in binding to TARPs, which are the auxiliary subunits of AMPARs. Arc, in a highly concentration-sensitive manner, acutely disperses TARPs from the postsynaptic density (PSD) condensate formed via phase separation. TARPs with the Ser residue in the “P-S-Y”-motif of its tail phosphorylated are completely refractory from being dispersed by Arc, suggesting that Arc cannot displace AMPARs from PSDs in active synapses. Conversely, strengthening the interaction between Arc and TARPs enhances Arc’s capacity in weakening synapses. Thus, Arc can specifically and effectively modulate synaptic AMPAR clustering via modulating PSD phase separation. Our study further suggests that activity-dependent, bi-directional modulation of PSD condensate formation/dispersion represents a general regulatory mechanism for synaptic plasticity.

Cell Research (2022) 32:914–930; <https://doi.org/10.1038/s41422-022-00697-9>

INTRODUCTION

The immediate early gene *Arc* (*arg3.1*) is one of the most sensitively regulated genes in neurons of living animals and in cultures in response to stimulations.^{1–6} Instead of being a transcription factor, *Arc* encodes a multidomain scaffold protein with its expression confined to brain and testis.⁷ In brain, *Arc* is exclusively expressed in CaMKII-positive glutamatergic neurons in neocortex and hippocampus.⁸ Upon stimulation, *Arc* protein can rapidly accumulate in postsynaptic protrusions including postsynaptic densities (PSDs) via local protein synthesis.^{2,9,10} Longer-term *Arc* synthesis requires transcription-mediated *Arc* mRNA expression.^{3,11,12} Synaptic *Arc* protein level is tightly regulated by ubiquitin-mediated *Arc* protein turnover and *Arc* mRNA degradation.^{13,14} Accumulation of *Arc* in a synapse leads to removal of AMPA receptors (AMPA) thus weakens the synapse.^{15–17} Such *Arc*-mediated synapse weakening has been implicated in multiple aspects of synaptic function, learning and memory including long-term depression, synaptic scaling, and memory storage.^{6,16–22} Both chronic and acute genetic removal of *Arc* in mice lead to various cognitive defects including spatial/contextual, emotional, and social memory deficits.^{19,21} Not surprisingly, deregulation of *Arc* has been implicated in neuronal disorders including fragile X syndrome, Angelman’s syndrome, schizophrenia and Alzheimer’s diseases among others.^{14,20,23,24}

Compelling evidence supports that synaptic *Arc* protein level is inversely correlated with synaptic AMPAR clustering. In cultured neurons, overexpression of *Arc* or activity-induced *Arc* level increase leads to decreased surface AMPAR level.^{9,15–17,25} Conversely, neurons derived from *Arc* KO mice have abnormally high

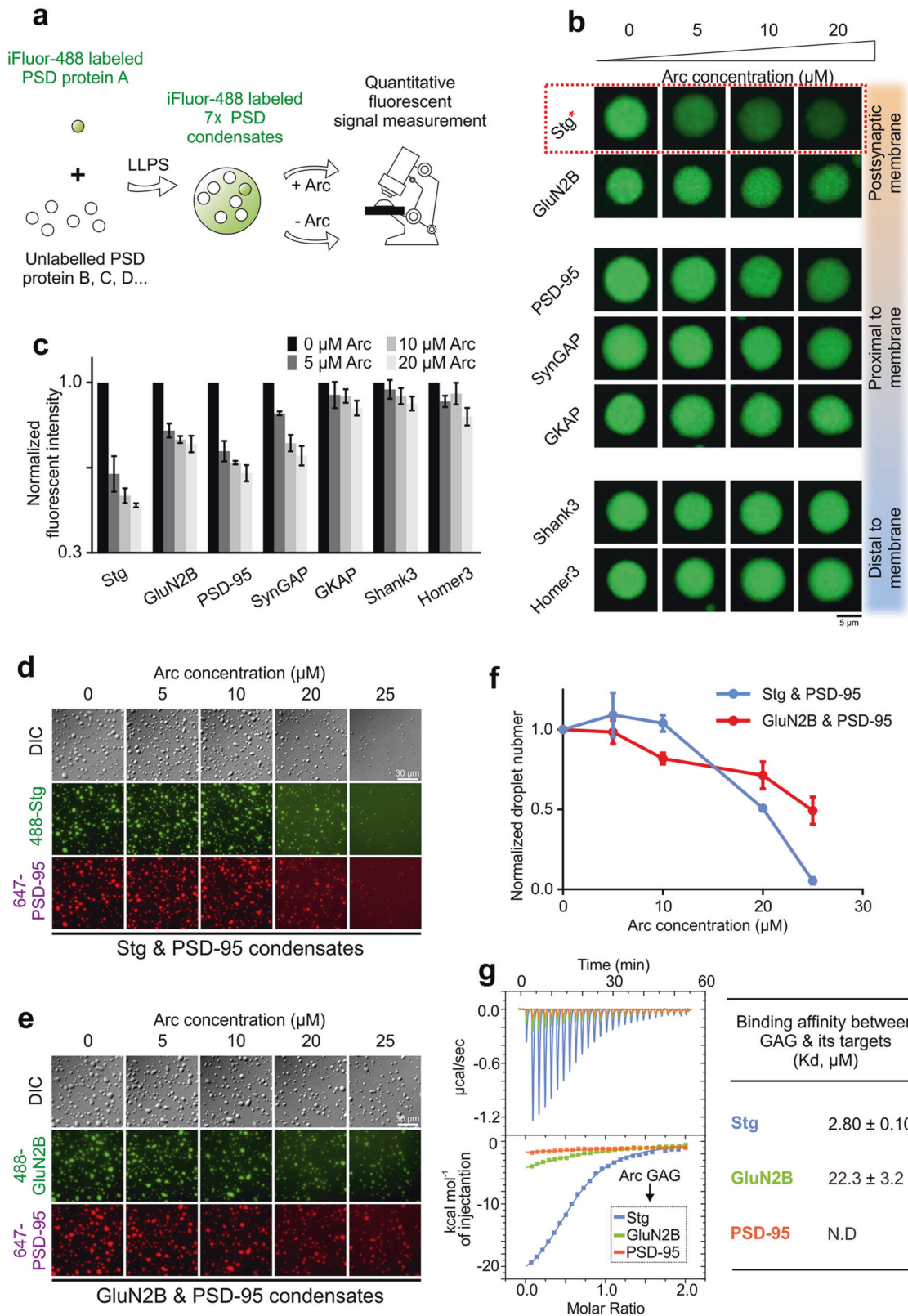
synaptic AMPARs and such neurons are defective in activity-induced AMPAR down-scaling.¹⁷ In vivo, *Arc* can coordinate local synaptic potentiation and depression by modulating redistribution of AMPARs between adjacent synapses on a dendritic spine.²⁶ Enrichment of *Arc* in inactive spines (also referred to as inverse tagging of synapses) is promoted by its interaction with inactive CaMKIIβ.⁹ Mechanistically, *Arc*-mediated removal of synaptic AMPAR is thought to occur via *Arc*-enhanced endocytosis of the receptors. *Arc* has been shown to bind to several proteins including endophilin, dynamin and AP-2 subunit, all of which are endocytic machinery proteins.^{15,27} However, it is unlikely that *Arc*-associated endocytic machinery can directly access synaptic AMPARs, which are insulated by the dense PSD assemblies. It is known that the endocytic zones of synapses are located outside of the PSD^{28,29} thus endocytic cargoes of synaptic proteins including AMPARs will need to be moved out of PSDs in order to be endocytosed. A recent study revealed that the N-lobe of *Arc* GAG domain can weakly but directly bind to several synaptic proteins including Stargazin, GluN2A/B, and GKAP, each containing a short “P-X-Y/F”-motif in their sequences,³⁰ although functional implications of *Arc*’s bindings to these proteins are not clear.

A series of our recent studies have provided evidence showing that PSDs are formed via liquid–liquid phase separation. Major PSD scaffold proteins including PSD-95, SAPAP, Shank and Homer interact with each other and with AMPARs forming intricate molecular assemblies via specific and multivalent interactions.^{31–34} Such PSD assemblies can autonomously form highly complex molecular networks and cluster AMPARs on lipid membranes. The PSD assembly formed via phase separation can be dispersed or

¹Division of Life Science, Hong Kong University of Science and Technology, Clear Water Bay, Kowloon, Hong Kong, China. ²Department of Neuroscience and Kavli Neuroscience Discovery Institute, Johns Hopkins University School of Medicine, Baltimore, MD, USA. ³School of Life Sciences, Southern University of Science and Technology, Shenzhen, Guangdong, China. ⁴These authors contributed equally: Xudong Chen, Bowen Jia. ✉email: zhangmj@sustech.edu.cn

Received: 30 November 2021 Accepted: 29 June 2022

Published online: 18 July 2022



enhanced by molecular events that are closely associated with synaptic activities. For example, the PSD network complexity as well as AMPAR cluster size is bi-directionally regulated by the abundance of major scaffold proteins such as PSD-95 or Shank

(i.e., higher level of scaffold proteins promotes PSD assembly and vice versa). Homer 1a, which is also the product of an immediate early gene and its expression level in neurons oscillates between sleep-wake cycle,³⁵ can effectively modulate PSD assembly

Fig. 1 Arc selectively disperses Stargazin in reconstituted PSD condensates. **a** Schematic diagram illustrating the imaging-based assay to screen specific synaptic targets of Arc by using reconstituted PSD condensates. In each imaging experiment, only one protein was sparsely labeled (at 2%) with iFluor-488. Unless otherwise specified, fluorescence labeling of proteins was at the 2% level throughout the study. **b** Confocal microscope images showing the enrichments of iFluor-488 proteins in 7× PSD droplets during Arc titration. **c** Quantitative analysis showing the enrichment changes of each PSD component during Arc titration. The fluorescent intensities of the protein in each titration were normalized to that obtained in the absence of Arc. Results were from three independent batches of imaging assays and presented as means ± SD. **d** DIC and fluorescence images showing the dispersion of the Stg/PSD-95 (15:5 μM) condensates by Arc. Results were from three independent batches of imaging assays and presented as means ± SD. **e** DIC and fluorescence images showing that Arc cannot disperse the GluN2B/PSD-95 (15:5 μM) condensates. **f** Quantification data showing the droplet numbers formed by Stg and PSD-95 in **d** and by GluN2B/PSD-95 in **e** during the Arc titrations. At each titration point, the droplet number was normalized to that obtained in the absence of Arc. Results were from three independent batches of imaging assays and presented as means ± SD. **g** ITC-based measurements comparing Arc's binding to Stg, GluN2B and PSD-95. 200 μM Arc GAG domain in syringe was titrated to 20 μM Stg, GluN2B and PSD-95, respectively, in reaction cell.

formation via antagonizing the tetrameric isoforms of the Homer family scaffolds.³¹ The PSD condensate, due to its unique organization nature afforded by phase separation, is ideally suited for rapid, activity-dependent, and bi-directional modulations of glutamate receptor clustering in synapses.^{34,36}

We hypothesize that Arc, being a cytosolic protein enriched in the PSD, is an ideal molecule to modulate the PSD condensate formation and AMPAR clustering in response to neuronal stimulations for the following several reasons. First, phase separation of the PSD condensate is highly sensitive to the concentration of each component within the PSD molecular network and Arc exhibits rapid and highly dynamic activity-dependent protein level changes in synapses. Second, extensive studies have established that the Arc protein level in synapses is intimately linked to synaptic activities. Third, Arc directly binds to the AMPAR auxiliary subunit TARPs including Stargazin, and thus Arc may modulate the PSD condensate network in a concentration-dependent manner. We tested our hypothesis in this study. We demonstrate that an elongated sequence from the tail of TARPs binds to both the N- and C-lobe of Arc GAG domain with an affinity much higher than previously identified interactions between “P-S-Y”-motif peptides and Arc. Arc directly antagonizes the interaction between PSD-95 and TARPs because the Arc-binding region and the PSD-95-binding region on TARPs overlap with each other. Importantly, Arc at its physiologically relevant concentration level can effectively disperse AMPARs from the PSD condensate. Thus, Arc may facilitate synaptic AMPAR removal by dispersing the receptors from PSD for subsequent endocytic removal.

RESULTS

Arc selectively disperses Stargazin in reconstituted PSD condensates

To investigate possible roles of Arc in modulating PSD assembly, we took advantage of the reconstituted PSD condensates with slight modifications.^{31,32} In addition to the scaffold proteins including PSD-95, GKAP, Shank3 and Homer3 and a synaptic enzyme SynGAP, we have also included the entire cytoplasmic tail of Stargazin (referred to as Stg from hereon) and a long fragment of GluN2B C-terminal tail in the reconstituted PSD system studied here (Fig. 1a and Supplementary information, Fig. S1). The Stg and the GluN2B C-terminal tail (termed as GluN2B in the following) were used as proxies of AMPARs and NMDARs, respectively, for probing their interactions with the PSD condensates. This seven-protein mixture, named as “7× PSD”, formed PSD condensates via phase separation with all seven proteins massively concentrated in the condensed phase (the far-left panels of images in Fig. 1b).

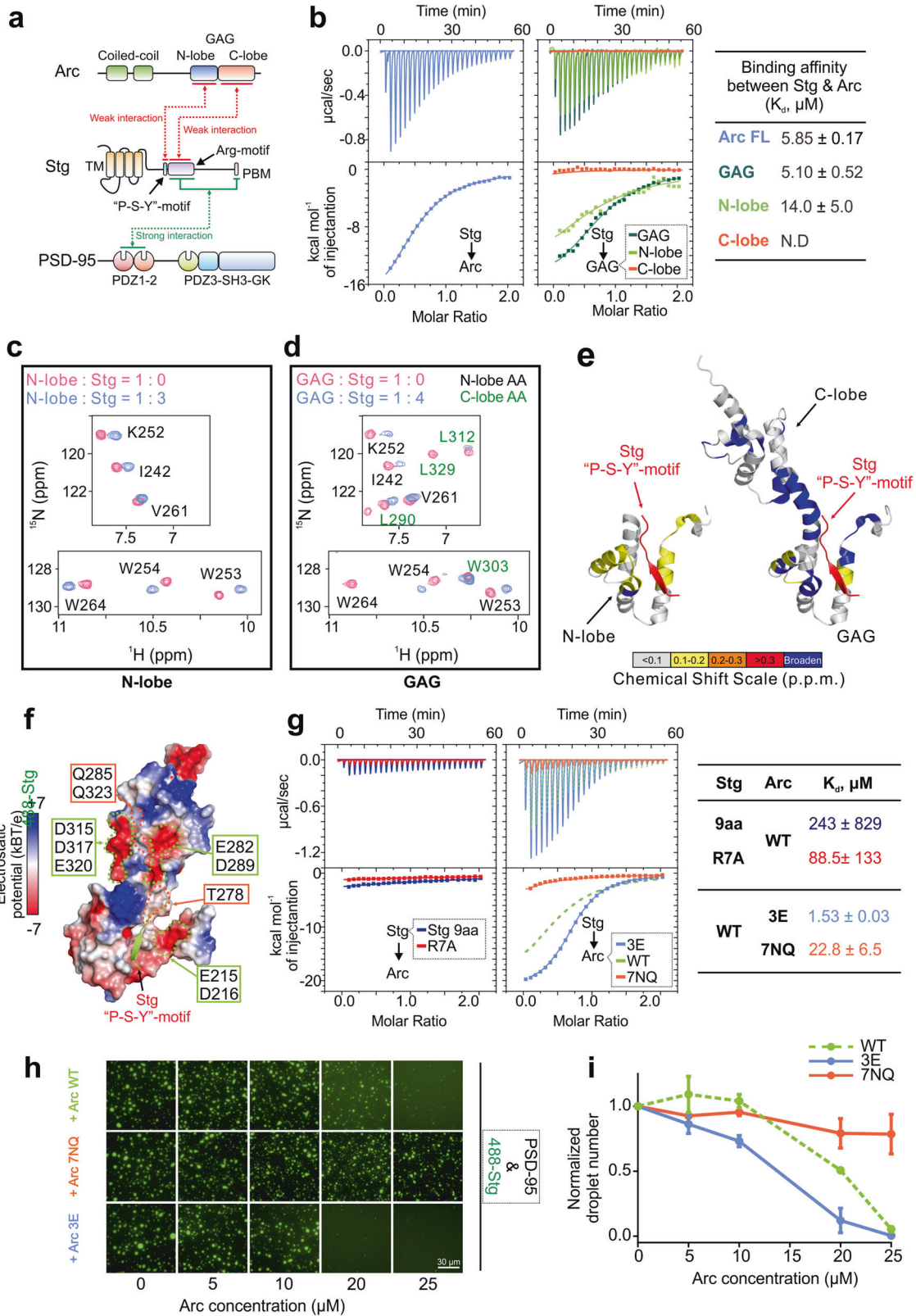
Next, we tested potential regulatory roles of Arc on the PSD assembly using the “7× PSD” system by increasing concentrations of purified full-length Arc protein, a process mimicking acute Arc concentration increase in synapses. To avoid possible imaging artifacts from signal crosstalk between different fluorophores, only one PSD component in the “7× PSD” system was sparsely labeled

with iFluor-488 dye in each titration, so that seven parallel titration experiments were performed in order to measure the impact of Arc on the assembly of each component into the PSD condensate (Fig. 1a). During the titration, the concentration of each component in the “7× PSD” system was fixed at 5 μM and Arc was increased from 0 to 20 μM. The fluorescence signal of each component was recorded by confocal microscope under the identical imaging setting (Fig. 1a). Increasing the concentration of Arc selectively reduced the enrichments of Stg, GluN2B, PSD-95 and SynGAP, all of which are the upper layer PSD proteins. In contrast, the PSD condensate enrichments of the lower layer of PSD scaffold proteins including GKAP, Shank3 and Homer3, were not affected by Arc (Fig. 1b, c). Among the upper layer proteins that were dispersed from PSD condensates by Arc, Stg showed its exquisite sensitivity to Arc concentration. For example, addition of an equal molar amount of Arc (5 μM) led to dispersion of >50% of Stg from the PSD condensates (Fig. 1c), suggesting that Stg may be a specific synaptic target of Arc.

As Stg and GluN2B can individually undergo phase separation and form stable condensates with PSD-95,^{32,37} we moved to the “2× PSD” systems (the Stg/PSD-95 condensate and the GluN2B/PSD-95 condensate) to dissect the mechanism underlying Arc-induced molecular component dispersions from the PSD condensates. Like the results from the “7× PSD” system, we observed a sharp, Arc concentration-dependent dispersion of the Stg/PSD-95 condensates formation during the Arc titration (Fig. 1d, quantified in 1f). In contrast, the impact of Arc on the GluN2B/PSD-95 condensate was milder and roughly linearly proportional to the Arc concentration, implying a rather non-specific impact of Arc on the system (Fig. 1e, f). Our above finding nicely correlates with previous discoveries showing that overexpression of Arc in cultured neurons selectively decreased synaptic AMPAR level but had no impact on synaptic NMDARs.¹⁶ It is noted that, in our in vitro reconstituted PSDs, Arc alone is sufficient (i.e., in the absence of any endocytic elements) to disperse Stg from the PSD condensates. Quantitative binding experiments revealed that the Arc GAG domain specifically binds to Stg with a medium-to-strong affinity ($K_d \sim 2.80 \mu\text{M}$). Whereas Arc showed a much weaker binding to GluN2B ($K_d \sim 22.3 \mu\text{M}$) and had no detectable binding to PSD-95 (Fig. 1g; see Fig. 2a for schematics of protein/protein interactions). Thus, it appears that, via direct and specific binding, Arc can disperse Stg from the PSD condensates.

Molecular determinants of Arc–Stg interaction

Next, we delineated the detailed molecular mechanism underlying the specific interaction between Arc and Stg. Arc is a multidomain protein composed of two N-terminal coiled-coil domains, a central unstructured linker, and a C-terminal conserved GAG domain, which can be further divided into N-lobe and C-lobe (Fig. 2a). Recent structural studies revealed that Arc uses the N-lobe of its GAG domain to bind to a short “P-X-Y/F”-motif containing synaptic proteins including Stg, GluN2A/2B, CaMKIIα and IQSEC2.^{30,38} The binding affinity of GAG to a hydrophobic dye-labeled Stg peptide (RIPSYR) is around $60 \mu\text{M}$ ³⁰ and to an unlabeled and slightly longer peptide (RIPSYRYRY) is about $240 \mu\text{M}$ (see Fig. 2g below). In



contrast, the full-length Arc or its GAG domain binds to Stg with a much stronger affinity ($K_d \sim 5\text{--}6 \mu\text{M}$; Fig. 2b), indicating that the C-lobe of GAG is also involved in binding to region(s) of Stg outside its "P-S-Y"-motif.

Truncation-based mapping experiments revealed that the N-lobe of GAG alone showed a ~ 3 -fold weakening in binding to Stg, whereas the C-lobe alone had no detectable binding by the ITC experiment (Fig. 2b), indicating that the N-lobe of GAG is the

Fig. 2 The mechanism underlying the interaction between Stg and Arc. **a** Schematic diagram showing the domain organizations of Arc, Stargazin and PSD-95. The interaction mode between Arc and Stargazin revealed in this study is marked in red line. The binding mode between PSD-95 and Stargazin characterized previously³² is marked in green line. **b** ITC-based measurements comparing Stg's binding to Arc, GAG, and the N-lobe and C-lobe of GAG. 200 μM Stg in syringe was titrated to 20 μM individual proteins indicated above. **c** Selected regions of the $^1\text{H}, ^{15}\text{N}$ HSQC spectra of GAG N-lobe with or without addition of an excess amount of Stg (see Supplementary information, Fig. S2a for the full spectra). **d** Selected regions of the $^1\text{H}, ^{15}\text{N}$ HSQC spectra of the GAG domain with or without addition an excess amount Stg. Residues corresponding to the GAG C-lobe are colored in green. (see Supplementary information, Fig. S2b for the full spectra.). **e** Mapping of the backbone amide chemical shift changes of N-lobe (left) or GAG (right) induced by Stg binding to their respective structures (see Supplementary information, Fig. S2 for details). **f** Surface representation showing the electrostatic potential of GAG contoured at ± 7 kT/e. Mutations in Arc 7NQ and Arc 3E are indicated in green and orange boxes, respectively (also see Supplementary information, Fig. S5b). **g** Left: ITC-based measurements showing Arc's binding to Stg 9aa and Stg R7A. 200 μM Stg 9aa or Stg R7A in syringe was titrated to 20 μM Arc. Middle: Comparisons of Stg's binding to Arc 7NQ and Arc 3E. 200 μM Stg in syringe was titrated to 20 μM each indicated Arc mutant. Right: the measured K_d values. **h** Fluorescence images showing the phase separation of Stg and PSD-95 in the presence of Arc 3E or Arc 7NQ. 15 μM Stg and 5 μM PSD-95 were pre-mixed for condensation, followed by the addition of individual Arc mutant with indicated concentration. Note that the images of Arc WT (top row) are the same as those in the middle row of Fig. 1d, as these are from the same experiment and Arc WT serves as the control for comparing the results from the two panels. **i** Quantification data showing the droplet numbers formed by Stg and PSD-95 in **h**. Results were from three independent batches of imaging assays and presented as means \pm SD. Again, the quantification for "WT" is the same as the curve of "Stg & PSD-95" in Fig. 1f.

primary binding site for Stg and the C-lobe plays an auxiliary role in enhancing Arc's binding to Stg.

We used NMR spectroscopy to visualize the binding of both N- and C-lobe of the Arc GAG domain to Stg. Titrating Stg to the ^{15}N -labeled GAG N-lobe induced specific chemical changes to the residues in the Stg "P-S-Y"-motif binding pocket of the N-lobe (Fig. 2c, e, left), which is in line with the reported structural studies.^{30,38} Notably, in addition to chemical shift changes in the N-lobe, titrating Stg to the ^{15}N -labeled GAG domain induced peak broadening of many residues in different sub-regions in the C-lobe (Fig. 2d, e; Supplementary information, Fig. S2a, b), indicating that the C-lobe of GAG weakly interacts with residues C-terminal to the "P-S-Y"-motif in Stg (Fig. 2e). Consistent with binding strengths of various Arc fragments to Stg (i.e., GAG > N-lobe > C-lobe), the GAG domain of Arc robustly dispersed condensates formed by PSD-95 and Stg, whereas the C-lobe only showed a mild effect (Supplementary information, Fig. S3a, b), although the full-length Arc and GAG display same affinity in binding to Stg (Fig. 2b). This is likely due to increased avidity of the full-length Arc in binding to Stg caused by dimerization of Arc by its the N-terminal coiled-coil domain.

The C-lobe of the Arc GAG domain contains two negatively charged surfaces that are juxtaposed to the Stg "P-S-Y"-motif binding pocket of the N-lobe (Fig. 2f).³⁸ Importantly, the "P-S-Y"-motif of Stg is immediately followed by a stretch of Arg residues (7 conserved Arg residues referred to as the Arg-motif; Figs. 2a and 3a). Thus, the charge-charge interaction between the Arg-motif of Stg and the C-lobe of GAG enhances the overall binding as well as the interaction specificity between Arc and Stg. We validated the above analysis with biochemistry experiments.

First, a short 9-residue peptide containing the "P-S-Y"-motif of Stg (Stg 9aa, 225-RIPSYRYRY-233) showed a remarkably weak affinity in binding to Arc ($K_d \sim 240 \mu\text{M}$; Fig. 2g), indicating that the short "P-S-Y"-motif alone is not sufficient for Stg to bind to Arc. Second, neutralization of seven Arg residues in the Stg Arg-motif with Ala (R230, R232, R235, R236, R238, R242, R250 to A, termed as Stg R7A) also dramatically weakened the interaction between Arc and Stg ($K_d \sim 90 \mu\text{M}$; Fig. 2g), confirming that the Arg-motif of Stg is indispensable for the interaction between Arc and Stg. Consistently, NMR-based titration experiments revealed that, compared to Stg WT, the Stg R7A mutant showed dramatically weakened chemical shift perturbation to the ^{15}N -GAG domain (Supplementary information, Fig. S4). In particular, there was no detectable chemical shift perturbations to the residues in the C-lobe of GAG when titrating with Stg R7A (Supplementary information, Fig. S4c), further supporting that the Arg-motif of Stg

interacts with the C-lobe of GAG. Third, neutralizing the negatively charged surfaces on the GAG domain by replacing seven exposed Glu and Asp with Gln and Asn, respectively (E215Q, D216N, E282Q, D289N, D315N, D317N, E320Q, named as Arc 7NQ; Supplementary information, Fig. S5a) weakened the binding between Arc and Stg (Fig. 2f, g and Supplementary information, Fig. S5b). Conversely, further increasing the negative charge density in the regions near the negatively charged surfaces of the GAG C-lobe by introducing three extra Glu residues (by replacing T278, Q285, and Q323 with Glu and the mutant is donated as Arc 3E; Fig. 2f and Supplementary information, Fig. S5b) led to several fold enhancement on the Arc/Stg interaction (Fig. 2g). Fully consistent with the above binding experiments, Arc 7NQ was much less capable of dispersing the Stg/PSD-95 condensates, whereas the Arc 3E mutant was even more potent than the WT protein in dispersing the Stg/PSD-95 condensates (Fig. 2h, i). By comparing the circular dichroism (CD) spectrum of each mutant with that of WT Arc, we concluded that the mutations introduced to Arc 7NQ or Arc 3E did not alter the overall folding of the protein (Supplementary information, Fig. S5c–e).

Taken together, our above biochemical studies have revealed a revised binding mode between Arc and Stg as illustrated in Fig. 2a. The "P-S-Y"-motif and the following Arg-motif bind to the N- and C-lobe of Arc GAG domain, respectively. The two binding sites together generate specific and strong interaction between Arc and Stg. Importantly, we showed recently that the Arg-motif of Stg is also critical for binding to PSD-95.³² Thus, the Arc dosage-dependent PSD condensate dispersion observed in Fig. 1 is likely mediated by a direct competition of Arc with PSD-95 for binding to Stg. Since the Stg/PSD-95 interaction (or interactions between TARPs and MAGUKs) is critical for AMPAR synaptic clustering via phase separation,³² Arc can act as an effective regulator in modulating AMPAR synaptic clustering by competing with PSD-95 for Stg and thus dispersing AMPARs from the PSD condensate.

Phosphorylation of S228 in the "P-S-Y"-motif of Stg renders the PSD condensate insensitive to Arc

Stargazin, as well as other TARP family members such as TARP γ -8, undergoes extensive activity-dependent phosphorylation.^{39–42} Ser residues within the cassette containing the "P-S-Y"-motif and the Arg-motif (Fig. 3a) are prime phosphorylation sites.⁴² Phosphorylation in this region is reported to modulate TARPs interactions with both phospholipids and PSD-95 and in turn regulates synaptic targeting of AMPARs.^{32,41,43} There are nine Ser residues in the Stg cassette, with one located in the "P-S-Y"-motif and the rest scattered along the Arg-motif (Fig. 3a).

To verify whether Stg phosphorylation changes its interaction with Arc, we generated nine different Stg variants each with

Fig. 3 Phosphorylation of S228 in the “P-S-Y”-motif of Stg renders PSD condensates insensitive to Arc. **a** Sequence alignment showing conserved motifs identified in the cytoplasmic tails of the TARP family members. Featured motifs are denoted by colored circles and triangles as indicated. H Homo sapiens, m Mus musculus. **b** Fluorescence images showing the phase separation of PSD-95 with individual Stg Ser-to-Asp variants without (up) or with addition of Arc (down). 15 μ M individual Stg mutant and 5 μ M PSD-95 were pre-mixed and 20 μ M Arc was added for dispersion. **c** Quantification data showing the droplet numbers formed by PSD-95 and each individual Stg mutant in (b). Results were from three independent batches of imaging assays and presented as means \pm SD. **d** ITC-based measurements showing Arc’s binding to different Stg phosphorylation-mimicking variants. 200 μ M individual Stg mutant in syringe was titrated to 20 μ M Arc. **e** Table summarizing K_d values of each Stg variant binding to Arc (green) or to PSD-95 (pink). **f** Schematic diagram illustrating the imaging assay to simultaneously visualize Arc-mediated dispersion of Stg WT, Stg S228D, and GluN2B. For PSD reconstitutions, 2.5 μ M Stg WT, 2.5 μ M Stg S228D and 5 μ M GluN2B were mixed with 4 \times PSD condensates formed by PSD-95, GKAP, Shank3 and Homer3 (each at 5 μ M). **g** Confocal microscope images showing the droplet enrichment changes of Stg WT, Stg-S228D and GluN2B in the PSD condensates as a function of Arc concentration. **h** Quantification of data in g showing the enrichment changes of Stg WT, Stg-S228D and GluN2B during Arc titration. Results were from three independent batches of imaging assays and presented as means \pm SD.

that none of these nine Stg mutants had any impact on Stg’s binding to PSD-95 (Fig. 3e and Supplementary information, Fig. S6). Finally, using synthetic phospho-Stg peptides, we showed that phosphorylation of Ser228 prevented Stg from being dispersed by Arc from the Stg/PSD-95 condensates. In contrast, Arc could effectively disperse Ser237 phosphorylated Stg from the Stg/PSD-95 condensates (Supplementary information, Fig. S7).

Then we used our “7 \times PSD” reconstitution system to test whether Arc might selectively disperse Stg from the PSD condensates. In this assay, we mixed equal amount of Stg WT and Stg S228D with GluN2B, PSD-95, SynGAP, GKAP, Shank3 and Homer3. We simultaneously labeled GluN2B, Stg WT and S228D with different dyes and recorded the fluorescent intensities of each protein in droplets during the Arc titration (Fig. 3f). As expected, Stg WT was potently dispersed by Arc. In contrast, Stg S228D, much like GluN2B, was resistant from being dispersed by Arc (Fig. 3g, h).

In summary, we discovered that phosphorylation of Ser228 in Stg can specifically weaken its binding to Arc but not to PSD-95. Thus, phosphorylation of Ser228 can essentially eliminate Arc’s capacity in dispersing Stg from the PSD condensate. This finding may be directly linked to well established observation that Arc selectively down-regulates AMPAR level in inactive synapses.⁹ We picture that phosphorylation of Ser228 of Stg does not occur in inactive synapses and thus Arc enrichment in such synapses (e.g., via binding to inactive CaMKII) can effectively disperse AMPARs from PSD for subsequent endocytosis.

Arc downregulates Stg and TARP γ -8, but not TARP γ -3

In TARPs, the Ser in the “P-S-Y”-motif is conserved among Stargazin, TARP γ -4 and TARP γ -8, but not in TARP γ -3, which is a Pro instead (Fig. 3a). The “P-S-Y”-motif on Stargazin forms a β -strand upon binding to the GAG N-lobe.³⁰ With Pro in the “P-X-Y”-motif is expected to dramatically weaken TARP γ -3’s binding to Arc. We tested this hypothesis by performing quantitative ITC-based binding measurements between the GAG domain and the entire cytoplasmic tail of both TARP γ -8 and TARP γ -3 (termed as γ -8 and γ -3 from hereon). Similar to Stg, γ -8 was found to bind to Arc with high affinity. In fact, the binding between Arc and γ -8 is slightly stronger than that between Arc and Stg (Fig. 4a). In contrast, γ -3 showed a very weak binding ($K_d > 60 \mu$ M) to Arc. Notably, replacing Pro226 (the Pro in the “P-P-Y”-motif) with Ser converted γ -3 into a strong Arc binder (Fig. 4a).

Totally consistent with the above biochemical analysis, Arc could very effectively disperse the γ -8/PSD-95 condensates, likely due to its stronger binding to Arc compared to other TARPs (Fig. 4b, c). In contrast, Arc could not disperse the γ -3/PSD-95 condensates. However, Arc could effectively disperse the condensates formed by the P226S mutant of γ -3 with PSD-95 (Fig. 4d, e).

Synapses in certain brain regions simultaneously express multiple isoforms of TARPs.^{44,45} We investigated whether Arc might display certain selectivity in dispersing different isoforms of TARPs from condensates formed by PSD scaffold proteins. We mixed Stg, γ -8 and γ -3 (each at 2.5 μ M and labeled with different fluorophores; Fig. 4f) with five other PSD components

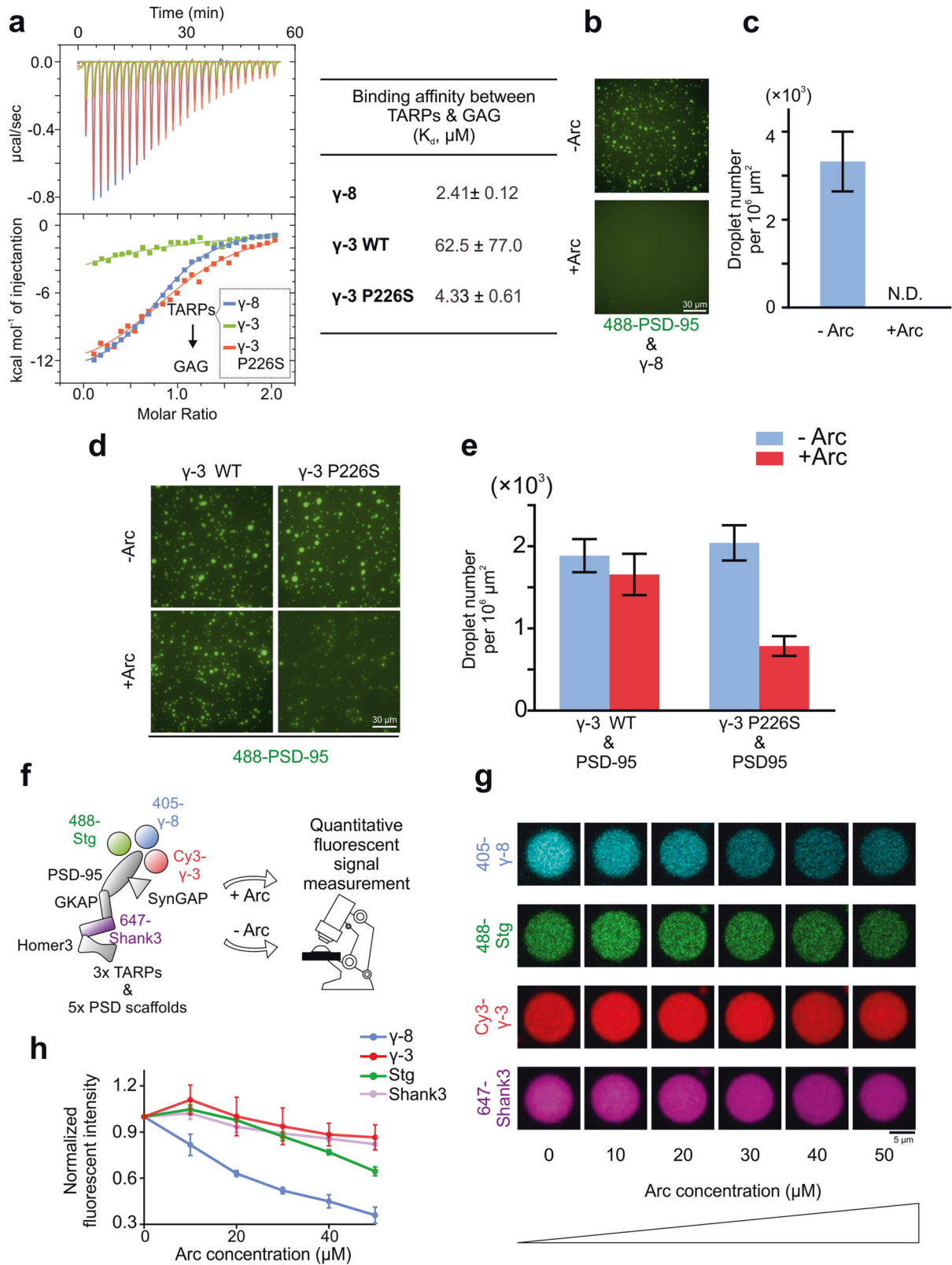
(PSD-95, SynGAP, GKAP, Shank3, and Homer3; each at 5 μ M, with Shank3 labeled with Alexa-647). In the absence of Arc, all three TARPs were highly concentrated in the reconstituted PSD condensates (Fig. 4g). We then titrated the PSD condensates with Arc and quantified the dispersion of each TARP from the PSD condensates as a function of increasing concentrations of Arc added. We discovered that γ -8, likely due to its strongest binding to Arc, was most effectively dispersed from PSD condensates by Arc. Stg could also be dispersed by Arc, though less effectively compared to γ -8. Arc could not disperse γ -3 from the PSD condensates (Fig. 4g, h). In fact, the enrichment of γ -3 in the PSD condensates was slightly increased upon Arc addition, likely due to additional binding slots freed up by dissociation of γ -8 and Stg from PSD-95. It is interesting to note that the dominant TARP isoform expressed in hippocampus of mice is γ -8, and the activity of hippocampal neurons is highly sensitive to the dosage of Arc.^{5,45–48}

Arc effectively disperses PSD condensate-mediated Stg clustering on lipid membranes

In synapses, the PSD is tethered to postsynaptic membranes by AMPARs and in return the PSD clusters AMPARs through direct TARP/MAGUK interactions. We showed that adding the PSD scaffold proteins to membrane-tethered Stg could be used as a proxy to study PSD formation and PSD-mediated AMPAR clustering on membrane surface via phase separation (Fig. 5a).^{31,32}

Consistent with our earlier findings, PSD components including PSD-95, GKAP, Shank3 and Homer3 (each in 1 μ M concentration) induced formation of sub-micron-sized clusters enriched with Stg on supported lipid bilayers (SLBs). The membrane clustering of Stg was progressively diminished when increasing amount of Arc was added (Fig. 5b). It is noted that in this membrane system, Arc could effectively disperse Stg clustering with Arc concentration as low as 0.5–1 μ M (Fig. 5b). We further investigated the capabilities of the Arc 3E and Arc 7NQ mutants in dispersing PSD condensate-mediated Stg clustering on membrane surface. Arc 3E was even more potent in dispersing Stg clustering than Arc WT did, whereas Arc 7NQ could not disperse Stg clustering on membrane surface (Fig. 5c, d).

Finally, we evaluated the clustering of the Stg S228D mutant on lipid membranes by the PSD condensates. On SLBs, Stg S228D formed clusters upon addition of PSD scaffold proteins as effectively as Stg WT did (Fig. 5e, f). Different from Stg WT, the clustered Stg S228D mutant could not be dispersed by Arc WT, Arc 3E, or Arc 7NQ (Fig. 5e, f), indicating that phosphorylation of Ser228 in the “P-S-Y”-motif of Stg does not impact its clustering by the PSD scaffold proteins on the membrane surface, but the formed Stg clusters are refractory from being dispersed by Arc. We repeated the same sets of the experiments shown in Fig. 5c–f but by replacing Stg with γ -8. Arc could effectively disperse γ -8 clustering induced by PSD condensates on membrane surface, but the PSD condensate-mediated clustering of γ -8 S264D (corresponding to S228D on Stg) could not be dispersed by Arc WT or Arc 3E (Supplementary information, Fig. S8).



Acute Arc concentration-dependent dispersion of Stg from the PSD condensate is a unique property manifested by phase separation

The biochemical data shown in Fig. 1 showed that the phase separation of PSD-95 and Stg is very sensitive to Arc concentration.

This is in apparent odd with the fact that PSD-95 binds to Stg with a ~10-fold higher affinity than Arc does to Stg (Fig. 6a). Following the equilibrium theory underlying the direct competition between Arc and PSD-95 in binding to Stg in dilute solution, Arc would need to be at concentrations much higher than that of PSD-95 in order

Fig. 4 Arc selectively disperses Stg and TARP γ -8, but not TARP γ -3, from the PSD condensates. **a** ITC-based measurements showing Arc's binding to γ -8, γ -3 WT, and γ -3 P226S. 200 μ M TARP_CT in syringe was titrated to 20 μ M Arc GAG. **b** Fluorescence images showing the phase separation of PSD-95 (5 μ M) and γ -8 (15 μ M) with or without addition of Arc (20 μ M). **c** Quantification data showing the droplet numbers formed by γ -8 and PSD-95 in **b**. Results were from 3 independent batches of imaging assays and presented as means \pm SD. **d** Fluorescence images showing the phase separation of PSD-95 (5 μ M) and γ -3 WT or γ -3 P226S (15 μ M) with or without addition of Arc (20 μ M). **e** Quantification data showing the droplet numbers formed by PSD-95 and γ -3 WT or γ -3 P226S in **d**. Results were from 3 independent batches of imaging assays and presented as means \pm SD. **f** Schematic diagram illustrating the imaging assay to simultaneously visualize Stg WT, γ -8, and γ -3 with increasing concentration of Arc. 2.5 μ M Stg, 2.5 μ M γ -8 and 2.5 μ M γ -3 were mixed with 4 \times PSD condensates formed by PSD-95, GKAP, Shank3 and Homer3 (each at 5 μ M). As high concentration of total TARPs led to heterogeneous distributions of different PSD proteins inside each single droplet (data not shown here), we used a special form of GKAP (with Ser-phosphorylation on the third GK-binding-repeat to enhance GKAP's association to PSD-95) to stabilize our reconstitution system thus allowing all the PSD proteins to perfectly colocalize.⁵³ **g** Confocal microscope images showing the droplet enrichment changes of Stg WT, γ -8, γ -3 and Shank3 in PSD droplets during the Arc titration. **h** Statistics analysis showing the enrichment changes of Stg WT, γ -8, γ -3 and Shank3 during the Arc titration in **g**. Results were from 3 independent batches of imaging assays and presented as means \pm SD.

to effectively disrupt the PSD-95/Stg complex. Thus, it appears that, in the condensed phase formed by phase separation, the competition between Arc and PSD-95 in binding to Stg does not follow the conventional equilibrium theory.

We designed another competition experiment to test this hypothesis. Mimicking protein concentrations in living synapses,⁴⁹ we fixed PSD-95 at 100 μ M and Stg at 25 μ M. Under this condition, Stg was saturated by PSD-95 and the mixture underwent phase separation to form highly dense PSD-95/Stg droplets (Fig. 6b). Next, we titrated Arc into this phase separated PSD-95/Stg mixture. Remarkably, Arc could disperse the PSD-95/Stg condensates with exquisite sensitivity (Fig. 6b, c). For example, in the presence of 10 μ M Arc (i.e., at a 2.5-fold lower concentration of Stg and only 1/10 of PSD-95), \sim 80% of PSD-95/Stg droplets were dispersed. We plotted the normalized number of PSD-95/Stg droplets as a function of the Arc concentration and observed a sharp Arc concentration-dependent dispersion curve for the PSD-95/Stg condensates (Fig. 6d, orange curve), reflecting a highly cooperative process for phase separation to occur or to disperse. In a stark contrast, if the competition between Arc and PSD-95 in binding to Stg follows the equilibrium theory in dilute solution (Fig. 6d, the simulated curve in blue), Arc-mediated PSD-95/Stg condensate dispersion barely begins at 100 μ M Arc and only \sim 50% of Stg would dissociate from PSD-95 when Arc reached 1000 μ M. Obviously, Arc would never reach such high concentration in synapses. Additionally, the simple competition model (i.e., the non-cooperative hyperbolic curve in blue, Fig. 6d) could not support acute Arc-concentration dependent dispersion of AMPARs from the PSD.

Hence, we propose that phase separation-mediated condensation of AMPARs (as the result of direct binding of TARPs to MAGUKs in the PSD condensate) not only allows stable localization and clustering of AMPARs at synapses, but also builds in unique regulatory mechanisms for dynamic regulations of AMPARs in response to different synaptic stimulations. In this study, we discovered that Arc can acutely and sensitively disperse the PSD condensate-mediated Stg clustering even though it binds to Stg weaker than PSD-95 does (Fig. 6e). Once dispersed from the condensed PSD, AMPARs can be effectively removed from synapses via endocytosis.¹⁵ Our finding is in line with numerous reported findings in the literature that Arc can acutely down-regulate synaptic AMPAR level and thus modulate synaptic plasticity.^{15,16} The model depicted in Fig. 6e further predicts that phase separation-mediated AMPAR clustering by the PSD condensate allows synapses to be sensitively (both in terms of time and by molecular components) and bi-directionally modulated by synaptic stimulations.

Arc disrupts synaptic localization of Stargazin via specific interaction

We next asked whether Arc modulates Stargazin synaptic targeting through the binding mode characterized by our biochemical studies. We transfected N-terminally GFP-tagged

Stargazin full-length (named as GFP-Stargazin) into mature primary hippocampal neurons (DIV16–18). GFP-Stargazin alone showed perfect synaptic localization indicated by GFP spine/shaft signal ratio (Fig. 7a, b). Next, full-length, WT Arc with a C-terminal mCherry tag was expressed to mimic Arc upregulation. The synaptic localization of GFP-Stargazin was impeded by the overexpression of Arc-mCherry (\sim 40% decrease compared to the control). Compared with WT, Arc-mCherry 3E was even more potent in dispersing GFP-Stargazin clustering in the synapses (\sim 70% decrease compared to the control). The loss-of-function mutant of Arc, Arc-mCherry 7NQ, instead showed no impact on the synaptic targeting and clustering of GFP-Stargazin (Fig. 7a, b).

We also tested how phosphorylation on Ser228 might potentially influence Arc-mediated Stargazin synaptic dispersion. We used GFP-Stargazin S228D mutant to mimic constitutive phosphorylation of Ser228 in its "P-S-Y"-motif. In parallel, we used GFP-Stargazin S228A mutant to mimic non-phosphorylated Stargazin. GFP-Stargazin S228A behaved similarly as GFP-Stargazin WT as it also underwent synaptic dispersion by Arc-mCherry WT and 3E but was refractory to the Arc 7NQ mutant (Fig. 7c, d). In contrast, GFP-Stargazin S228D, was resistant to the overexpression of the WT as well as all of three mutants of Arc (Fig. 7e, f). Taken together, the above neuronal culture experiments, together with in vitro biochemical studies, indicate that Arc-mediated Stargazin down-regulation from synapses is likely via specific interaction between Arc and Stargazin and its consequent dispersion from the PSD condensate.

Arc GAG domain is sufficient in dispersing Stargazin clustering in synapses

Arc facilitates AMPAR endocytosis in synapses via direct interaction with endophilin or dynamin.¹⁵ Our study above suggests that Arc down-regulates AMPAR clustering via dispersing its condensation in the PSD. We asked whether Arc-TARP interaction may affect its binding to the two endocytic proteins. We found that Arc GAG domain has no detectable binding to dynamin2 or to endophilin3 (Supplementary information, Fig. S9), suggesting that the Arc-TARP interaction is independent of the Arc-endocytic machineries interactions. To further delineate the mechanism underlying the Arc-mediated AMPAR removal from synapses, we tested whether the Arc GAG domain (i.e., an Arc mutant lacking endophilin binding) might be sufficient in down-regulating Stargazin synaptic clustering in cultured neurons. To simplify our assay system, we replaced the entire Stargazin extracellular and transmembrane domains with the single transmembrane helix from platelet-derived growth factor receptor (PDGFR) and the resulted construct was named as GFP-PDGFR-TM-Stg_CT. GFP-PDGFR-TM-Stg_CT was completely disassociated from the core AMPARs and thus avoided possible complications of its synaptic trafficking and clustering contributed by the receptor core subunits or other TARPs associated with the receptor core. As reported,⁵⁰ GFP-PDGFR-TM-Stg_CT was nicely trafficked to and

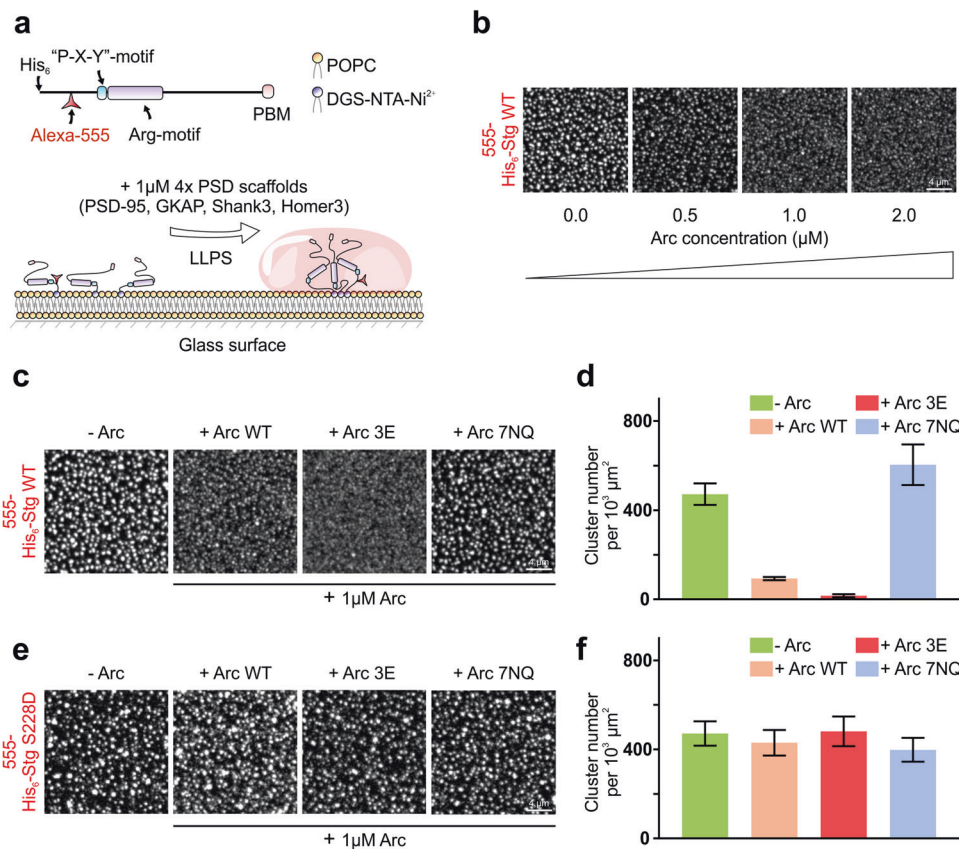


Fig. 5 Arc effectively disperses PSD condensate-mediated Stg clustering on lipid membranes. **a** Schematic diagram showing the clustering of Stg on SLBs by the PSD condensates formed by four scaffold proteins.³² In this assay, Stg was labeled with Alexa-555 at 5% for fluorescent imaging. **b** Confocal microscope images showing that the PSD condensate-mediated membrane clustering of Stg is progressively diminished upon addition of increasing amount of Arc. **c** Confocal microscope images showing the membrane clustering of Stg WT by the PSD condensates in the presence of Arc WT, Arc 3E and Arc 7NQ, respectively. **d** Statistics analysis showing the numbers of Stg clusters on SLBs in the presence of Arc or its variants as shown in **c**. Results were from 3 independent batches of imaging assays and presented as means \pm SD. **e** Confocal microscope images showing the membrane clustering of Stg S228D by the PSD condensates in the presence of Arc WT, Arc 3E and Arc 7NQ, respectively. **f** Statistics analysis showing the numbers of Stg S228D cluster on SLBs as shown in **e**. Results were from 3 independent batches of imaging assays and presented as means \pm SD. Scale bar, 4 μm.

clustered at synapses when expressed in hippocampal neurons (Fig. 8a, b), illustrating the critical roles of the Stg/PSD-95 interaction and phase separation in Stargazin's synaptic clustering.³² Expression of WT Arc GAG down-regulated GFP-PDGFR-TM-Stg_{CT} synaptic clustering. The GAG 3E mutant, which has an enhanced binding to Stg compared to WT GAG, was more potent in dispersing GFP-PDGFR-TM-Stg_{CT} synaptic clustering. Conversely, the GAG 7NQ mutant, which is defective in binding to Stg, was not effective in dispersing GFP-PDGFR-TM-Stg_{CT} synaptic clustering (Fig. 8a, b). We also constructed GFP-PDGFR-TM-Stg_{CT} S228D and S228A mutants to assay their dispersions by the Arc GAG. Similar to what was observed for the full-length Arc in Fig. 7, GFP-PDGFR-TM-Stg_{CT} S228A could be effectively dispersed by Arc GAG, whereas the GFP-PDGFR-TM-Stg_{CT} S228D mutant did not respond to the Arc GAG domain (Fig. 8c, d). The above experiments indicated that the binding between Arc GAG domain and the Stargazin tail is necessary and sufficient to disperse Stargazin from synapses. It should be noted that our experiment is not contradictory to endocytosis mediated AMPAR removal upon Arc increase in synapses. Dispersion of AMPARs from the PSD by Arc presumably moves PSD-clustered AMPARs to extra-synaptic regions of synapses, which become accessible to the endocytic machinery (Fig. 6e).

Finally, we tested whether the sensitive, Arc-dependent dispersion of Stg from the PSD-95/Stg condensates could occur in synapses using the simplified but highly specific GFP-PDGFR-

TM-Stg_{CT} and Arc GAG system. Overexpression of PSD-95 together with GFP-PDGFR-TM-Stg_{CT} led to enhanced synaptic clustering of GFP-PDGFR-TM-Stg_{CT} (Fig. 8a, b vs e, f), presumably due to enhanced PSD-95/Stg phase separation.^{31,32} Under this PSD-95 overexpression condition, GFP-PDGFR-TM-Stg_{CT} is likely saturated by PSD-95. If competition between Arc GAG and PSD-95 for GFP-PDGFR-TM-Stg_{CT} operated with the conventional equilibrium theory in dilute solution, Arc GAG would be very hard to compete with PSD-95 in binding to GFP-PDGFR-TM-Stg_{CT}. Our experiment suggested otherwise. WT Arc GAG could down-regulate synaptic clustering of GFP-PDGFR-TM-Stg_{CT} and the Arc GAG 3E mutant was more potent in doing so. In contrast, the Arc GAG 7NQ mutant was not capable of dispersing GFP-PDGFR-TM-Stg_{CT} clusters in synapses (Fig. 8e, f). Thus, the results presented in Figs. 7 and 8 support the model shown in Fig. 6e depicting Arc-mediated dispersion of Stg and hence likely AMPARs from the PSD condensate in synapses.

DISCUSSION

It is somewhat counter intuitive that Arc, one of most important memory-related genes rapidly and robustly induced by various neuronal activities,^{1,5,20,21} encodes a scaffold protein instead of a transcription factor. The best-known function of Arc is to acutely weaken synapses that are not stimulated (i.e., modulating Hebbian

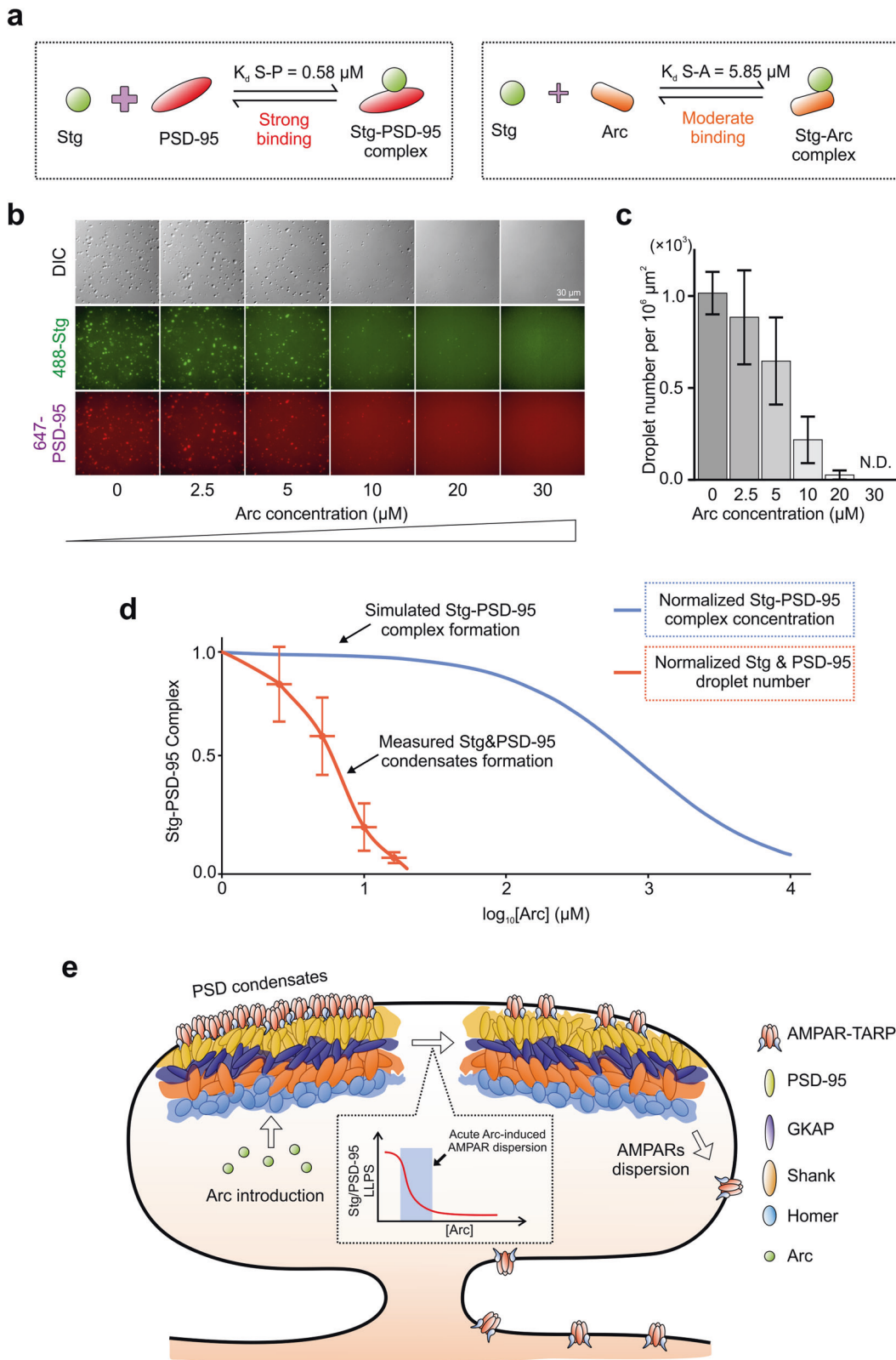
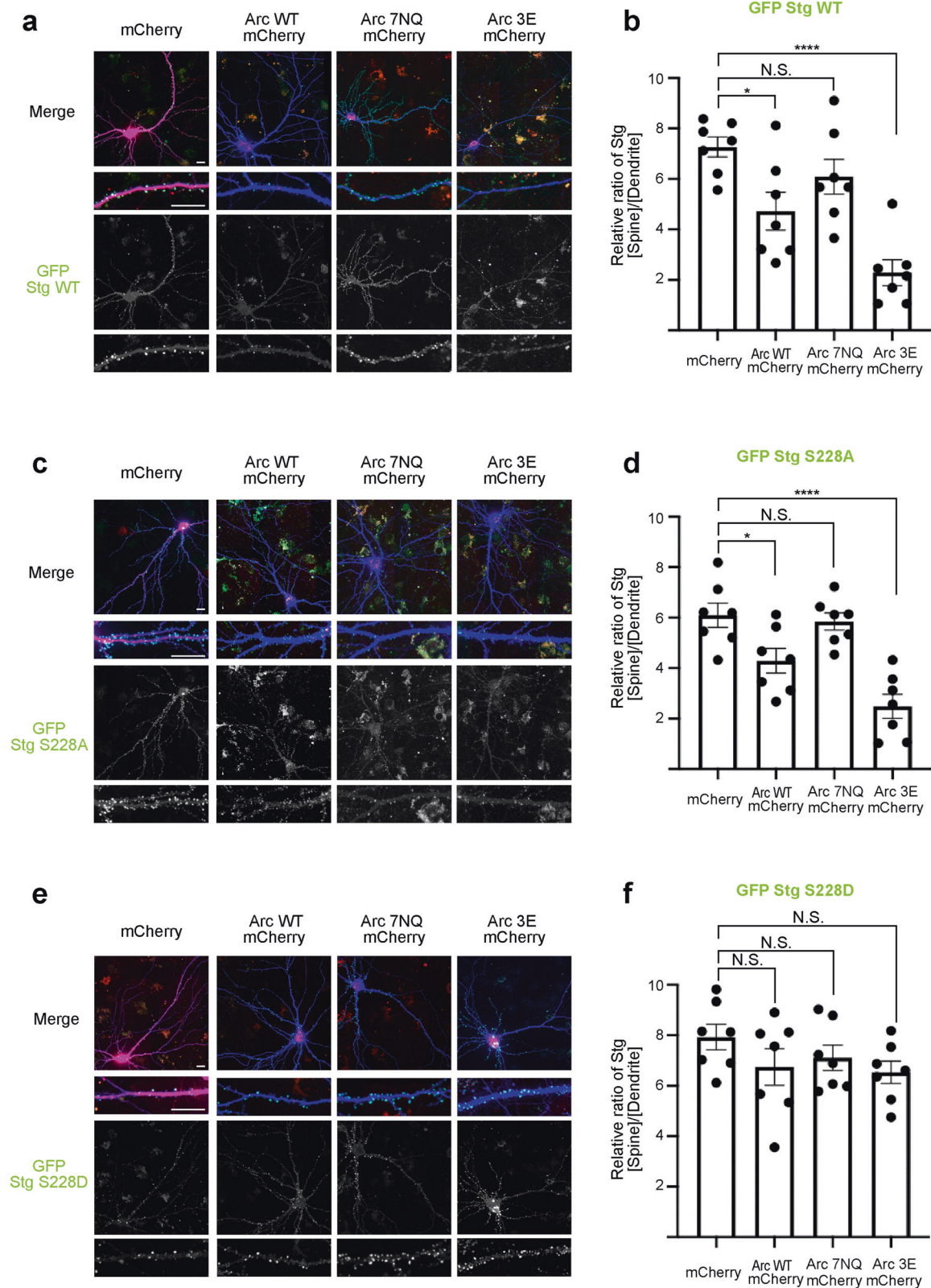


Fig. 6 Acute Arc concentration-dependent dispersion of Stg from the PSD condensates. **a** Schematic diagram showing the bindings of Stg to PSD-95 or Arc. **b** DIC and fluorescence images showing that low amount of Arc can effectively disperse the condensates formed by excessive amount of PSD-95 (100 μM) mixed with sub-stoichiometric amount of Stg (25 μM). **c** Quantification showing the droplet numbers formed by Stg and PSD-95 in **b**. **d** Plot of normalized droplet numbers formed by Stg and PSD-95 in **b** as the function of added Arc concentration (Orange curve). For comparison, a simulated plot showing fractions of Stg/PSD-95 complex existed in the mixture as the function of the added Arc assuming a simple competition between Arc and PSD-95 for binding to Stg (Blue curve). **e** A model depicting PSD condensate-mediated clustering of AMPARs in the PSD. Rise of Arc concentration can sensitively and cooperatively disperse AMPAR clustering via reversing phase separation of Stg and PSD-95. AMPARs dispersed from the PSD become accessible to synaptic endocytic machineries.



plasticity)⁹ or to scale down activities of synapses in neurons with high network activity (i.e., regulating homeostatic plasticity).¹⁷ Mechanistically, Arc is required for removal of synaptic AMPARs via endocytosis.¹⁵ Since the endocytic machinery is located outside the PSD where clustered AMPARs are situated, there

must be additional mechanism(s) underlying Arc-mediated synaptic AMPAR removal.

In this work, we discovered that via simultaneously binding to the "P-S-Y"-motif and the Arg-motif of the C-terminal tail of TARPs, Arc specifically and effectively competes with PSD-95 in binding to

Fig. 7 The specific Arc/Stg interaction is required for Arc-induced down-regulation of Stargazin from synapses. **a** Representative confocal images of cultured rat hippocampal neurons expressing GFP-Stargazin, and mCherry or individual mCherry-tagged Arc WT, Arc 3E and Arc 7NQ, respectively. **b** Quantification of averaged GFP-Stargazin spine/shaft intensity ratio on rat hippocampal neurons expressing individual Arc constructs. Error bars indicate \pm SEM. One-way ANOVA followed by Tukey's post hoc test, $n = 7$ neurons, 20–50 spines per neuron, $***P < 0.001$, $**P < 0.01$, $*P < 0.05$. **c** Representative confocal images of cultured rat hippocampal neurons expressing GFP-Stargazin S228A, and mCherry or individual mCherry-tagged Arc WT, Arc 3E and Arc 7NQ, respectively. **d** Quantification of averaged GFP-Stargazin S228A spine/shaft intensity ratio on rat hippocampal neurons expressing individual Arc constructs. Error bars indicate \pm SEM. One-way ANOVA followed by Tukey's post hoc test, $n = 7$ neurons, 20–50 spines per neuron, $***P < 0.001$, $**P < 0.01$, $*P < 0.05$. **e** Representative confocal images of cultured rat hippocampal neurons expressing GFP-Stargazin S228D, and mCherry or individual mCherry-tagged Arc WT, Arc 3E and Arc 7NQ, respectively. **f** Quantification of averaged GFP-Stargazin S228D spine/shaft intensity ratio on rat hippocampal neurons expressing individual Arc genes. Error bars indicate \pm SEM. One-way ANOVA followed by Tukey's post hoc test, $n = 7$ neurons, 20–50 spines per neuron, $***P < 0.001$, $**P < 0.01$, $*P < 0.05$. Scale bar, 20 μ m.

TARPs. Most importantly, due to this competition, Arc can disperse TARPs (and thus AMPARs) from being concentrated and clustered in the reconstituted PSD condensates, which are formed via liquid–liquid phase separation. This Arc-mediated TARP dispersion from PSD is exquisitely sensitive to the concentration of Arc, a finding that matches well with numerous previously studies of Arc-dependent AMPAR downscaling in cultured neurons and in neurons of living animals.^{15–17,20,26} One may envision that acute Arc protein level increase, via local mRNA translation and subsequent specific Arc protein enrichment in an unstimulated synapse,⁹ disperses AMPARs from the PSD condensates and facilitates the endocytosis of the dispersed receptors at the extra-synaptic sites. This acute Arc-mediated AMPAR dispersion from PSD may be a molecular mechanism underlying Arc's function in the Hebbian form of synaptic plasticity. Arc mRNA transcription is also known to be dramatically upregulated upon neuronal stimulations.^{1,3,5} There is a time-delay for Arc being translated from these newly transcribed messengers. It is possible that this form of Arc may be able to target synapses that were previously activated, thus leading to a global downscaling of these synapses, and thereby achieving Arc-mediated homeostatic synaptic scaling. It appears that the unique temporal regulations of Arc biogenesis and specific Arc enrichment into synapses at the basal state, both of which are tightly linked with different forms of neuronal stimulations, make the scaffold protein Arc ideal for modulating synaptic plasticity.

Synaptic strength is directly and almost linearly correlated with the physical size and PSD area of a synapse.⁵¹ We have demonstrated that phase separation likely underlies the formation of PSD and PSD-mediated clustering of glutamate receptors.^{31–34,37} Several hallmarks of phase separation-mediated formation of condensed molecular assemblies including PSDs are particularly attractive for activity-mediated synaptic plasticity. First, phase separation-mediated PSD formation is highly cooperative (i.e., with a switch-like property) and very sensitive to concentrations of protein components, meaning that synapse formation and growth or downsizing of synapses can be rapidly induced by neuronal activity. Second, modulations of PSD condensate formation or dispersion are also highly cooperative and follow yet still unknown mechanism(s) that is distinctly different from conventional equilibrium theory in dilute solutions. In this study, Arc can cooperatively and very effectively disperse TARPs from the PSD condensates in an Arc concentration range reachable in living neurons, although Arc binds to TARPs with a \sim 10-fold weaker affinity than PSD-95 does (Fig. 6). We showed in another example earlier that Homer1a, the product of another immediate early gene *Homer1a* and a synaptic scaffold protein, can effectively disperse the PSD condensates by acting on the Homer/Shank node of the entire PSD assembly network.³¹ We anticipate that the PSD condensate, a condensed molecular assembly falling into the regime of soft matter physics, will continue to offer many new properties that do not exist in the theoretical framework for dilution solutions. Third, PSD condensate formation and dispersion are very sensitive to activity-induced modifications of proteins. In this study, we showed that phosphorylation of the Ser residue in the "P-S-Y"-motif of TARP's tail

renders the PSD-clustered TARPs totally insensitive to Arc (Figs. 3 and 5). It is known that synaptic activation can lead to the phosphorylation of the Ser residue in the "P-S-Y"-motif of TARPs.⁴² Thus, TARP-bound AMPARs in active synapses are refractory to Arc-mediated downscaling. In contrast, synapses with basal activities can enrich Arc via binding to non-activated CaMKII β and subsequently enhance AMPAR removal by Arc-mediated dispersion from the PSD condensates. Conversely, in activated synapses, activation of CaMKII can effectively phosphorylate scaffold proteins including SAPAPs.⁵² Phosphorylation of SAPAPs dramatically enhances its binding to PSD-95, promotes phase separation of the PSD assembly, and enhances formation of synapses with larger spine heads.^{53,54} Thus, Arc can facilitate Hebbian strengthening of activated synapses and hetero-synaptic weakening of locally unstimulated synapses simultaneously.²⁶

We demonstrated that Arc shows very different binding affinities to the different isoforms of TARPs. It binds to TARP- γ 8 with the highest affinity, to Stargazin with a slightly weaker affinity, and almost no binding to TARP- γ 3. Interestingly, the binding affinities between TARPs and Arc are nicely correlated with the ability of Arc in dispersing TARPs from the PSD condensates (Fig. 4). Arc is most effective in dispersing TARP- γ 8 from PSD but not capable of doing so for TARP- γ 3. Different isoforms of TARPs are distinctly expressed in different brain regions.^{45,46} It is possible that AMPARs with different TARPs as auxiliary subunits may display different sensitivities to Arc in terms of Arc-mediated synaptic removal. It is noted that TARP- γ 8 is the dominant isoform of TARPs expressed in hippocampus in mice, and hippocampal neurons are very sensitive in responding to Arc level changes.

The TARP binding of Arc is likely an evolutionary gain of the function that is diverged from its ancient GAG domain-mediated capsid formation.^{55,56} Analytical ultracentrifuge (AUC) assay shows that, in the presence of TARP_CT, the full-length Arc cannot oligomerize but instead form a weak dimer in solution (Supplementary information, Fig. S10). It is noted that, from the capsid structure formed by *Drosophila* Arc, a short extension immediately preceding the N-terminal Arc GAG N-lobe binds to the same pocket as the "P-X-Y"-motif peptides do to the GAG N-lobe.^{30,38,57} This N-terminal extension of the GAG domain is critical for Arc capsid formation.⁵⁷ Displacement of this N-terminal extension from the Arc GAG N-lobe by TARP_CT provides an explanation to why the TARP-bound Arc cannot form oligomeric capsid structure.

In summary, we have provided evidence indicating that Arc, via directly binding to TARPs, may effectively disperse AMPARs from the PSD condensates formed via phase separation. Such Arc-mediated AMPAR dispersion from PSD may be a possible mechanism underlying how Arc, as a scaffold protein, can effectively modulate both Hebbian and homeostatic forms of synaptic plasticity.

METHOD DETAILS

Protein expression and purification

Sequences encoding various proteins were generated using standard PCR-based methods, each cloned into a vector

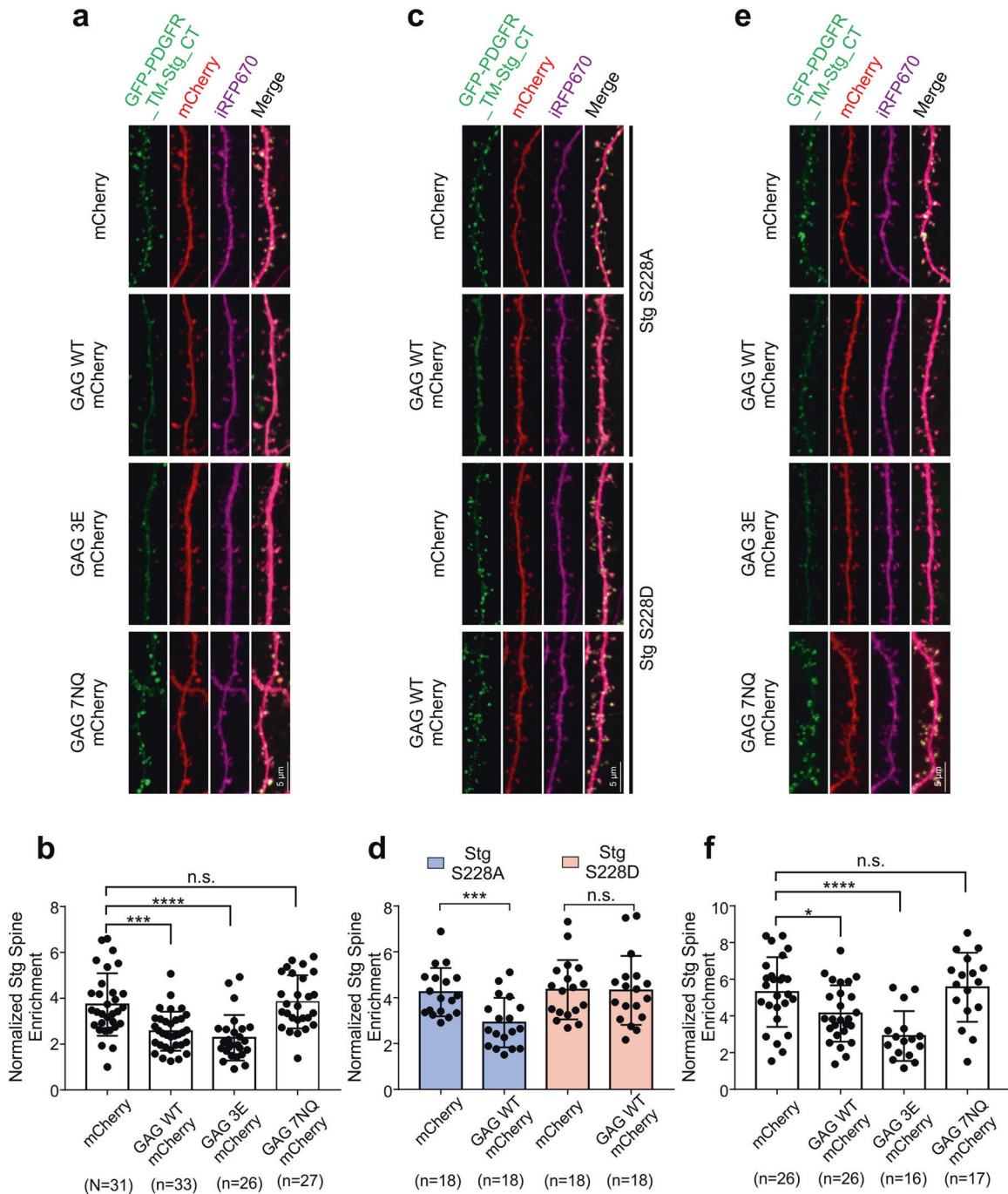


Fig. 8 The GAG domain of Arc is sufficient in dispersing Stargazin clusters in synapses. **a** Representative confocal images of cultured mouse hippocampal neurons expressing GFP-PDGFR-TM-Stg_CT WT, iRFP670 (as the cell fill), and mCherry or individual mCherry-tagged GAG WT, GAG 3E and GAG 7NQ, respectively. **b** Quantification of averaged GFP-PDGFR-TM-Stg_CT spine/shaft intensity ratios normalized with iRFP670 in mice hippocampal neurons expressing individual Arc constructs. Error bars indicate \pm SEM. One-way ANOVA followed by Tukey's post hoc test, "n" equals number of neurons with 20–30 spines per neuron, $***P < 0.001$, $**P < 0.01$, $*P < 0.05$. **c** Representative confocal images of cultured mouse hippocampal neurons expressing GFP-PDGFR-TM-Stg_CT S228A (up) or S228D (down), iRFP670, and mCherry or GAG-mCherry. **d** Quantification of averaged GFP-PDGFR-TM-Stg_CT S228A or S228D spine/shaft intensity ratios normalized with iRFP670 in mice hippocampal neurons expressing mCherry or GAG-mCherry. Error bars indicate \pm SEM. One-way ANOVA followed by Tukey's post hoc test, "n" equals number of neurons with 20–30 spines per neuron, $***P < 0.001$, $**P < 0.01$, $*P < 0.05$. **e** Representative confocal images of cultured mouse hippocampal neurons expressing GFP-PDGFR-TM-Stg_CT WT, iRFP670, PSD-95, and mCherry or individual mCherry-tagged GAG WT, GAG 3E and GAG 7NQ, respectively. **f** Quantification of averaged GFP-PDGFR-TM-Stg_CT spine/shaft intensity ratios normalized with iRFP670 in mice hippocampal neurons expressing individual Arc constructs. Error bars indicate \pm SEM. One-way ANOVA followed by Tukey's post hoc test, "n" equals number of neurons with 20–30 spines per neuron, $***P < 0.001$, $**P < 0.01$, $*P < 0.05$.

containing an N-terminal Trx-His₆ or a His₆-affinity tag followed by an HRV 3C cutting site. All constructs were confirmed by DNA sequencing. Recombinant proteins were expressed in *Escherichia coli* BL21-CodonPlus (DE3)-RIL (Agilent) in LB medium at 16 °C overnight and protein expression was induced by 0.25 mM IPTG (final concentration) at OD₆₀₀ between 0.6 and 0.8. Uniformly ¹⁵N-labeled GAG and GAG N-lobe for NMR analysis were prepared by growing bacteria in M9 minimal medium using ¹⁵NH₄Cl as the sole nitrogen source. Typically, each recombinant protein was purified using a nickel-NTA agarose affinity column followed by a size-exclusion chromatography (Superdex 200 or Superdex 75) with a column buffer containing 50 mM Tris, pH 8.0, 100 mM NaCl, 1 mM EDTA, 2 mM DTT.

For purifications of PSD-95 (UniProt: P78352-1) and Homer3 (UniProt: Q9NSC5-1), a mono Q ion-exchange chromatography was added to remove DNA contamination and degraded proteins after the size-exclusion chromatography by Superdex 200. After cleavage by HRV 3C protease, the Trx-His₆ or His₆-affinity tag was separated by another step of size-exclusion chromatography using Superdex 200 with the column buffer containing 50 mM Tris, pH 8.0, 100 mM NaCl, 1 mM EDTA, 2 mM DTT.

Stg (NCBI: NP_031609, 203D-323V), γ-8 (NCBI: NP_573453, 228E-423V, without Ala341-Ala349 in our template) and γ-3 (NCBI: NP_062303.2, 202E-315V), GluN2B (UniProt: Q00960, 1170G-1482V) were expressed at 37 °C for 3 h to minimize protein degradation. For γ-3 and GluN2B, 8 M urea was used during the Trx-His₆/His₆-affinity purification step. Urea was removed immediately after protein binding to the nickel-NTA agarose beads. Proteins eluted from the affinity column were then purified by Superdex 75 size-exclusion chromatography with a column buffer containing 50 mM Tris, pH 8.0, 300 mM NaCl, 1 mM EDTA, 2 mM DTT. After affinity tag cleavage by HRV 3C protease, a mono S ion-exchange chromatography was used to remove the Trx-His₆ tag and DNA contamination from TARP_CTs. Proteins were exchanged into a working buffer containing 50 mM Tris, pH 8.0, 100 mM NaCl, 1 mM EDTA, 2 mM DTT by a HiTrap desalting column.

Trx-His₆-3C-His₆-Stg and γ-8, as well as their Ser-to-Asp mutants, were expressed at 37 °C for 3 h and purified by nickel-NTA agarose affinity chromatography in the presence of 8 M urea, followed by Superdex 75 size-exclusion chromatography with a buffer containing 50 mM Tris, pH 8.0, 300 mM NaCl, 1 mM EDTA, 2 mM DTT. The affinity tag was cleaved by HRV 3C protease and removed by a step of mono S ion-exchange chromatography. Each purified protein was finally exchanged into a working buffer containing 50 mM Tris, pH 8.0, 300 mM NaCl, 1 mM TCEP by a HiTrap desalting column.

Protein fluorescence labeling

For amide labeling. Highly purified proteins were exchanged into a NaHCO₃ buffer (containing 100 mM NaHCO₃, pH 8.3, 300 mM NaCl, 1 mM EDTA and 2 mM DTT) and concentrated to 5–10 mg/mL. Alexa-647 NHS ester (Invitrogen) and iFluor-488/Cy3/iFluor-405 NHS ester (AAT Bioquest) were dissolved by DMSO making stock solutions at the concentration of 10 mg/mL. Each dye and the protein to be labeled were mixed at a molar ratio of 1:1 and the reaction was lasted for 1 h at room temperature. Reaction was quenched by 200 mM Tris, pH 8.2. The fluorophores and other small molecules were removed from the proteins by passing the reaction mixture through a HiTrap desalting column with buffer containing 50 mM Tris, pH 8.0, 100 mM NaCl, 1 mM EDTA and 2 mM DTT.

For cysteine labeling. His₆-Stg WT and S228D were labeled at a specific site away from the His₆-tag, the P-S-Y-motif, the Arg-motif and PBM in order to minimize any potential impact of the conjugated fluorophore on the binding of Stg to Arc or PSD-95. Cys302, which is adjacent to PBM of Stg, was substituted with Ser. Thr215 was then converted to Cys for the single site fluorophore conjugation. For His₆-γ-8 WT and His₆-γ-8 S264D, Cys235 was

substituted with Ser and Ser239 was converted to Cys for fluorescence labeling. The resulting His₆-Stg and His₆-γ-8 (WT and mutants) were each prepared in a labeling buffer (50 mM Tris, pH 7.5, 300 mM NaCl, 1 mM EDTA and 1 mM TCEP) with final concentration of 2 mg/mL. iFluor-555 maleimide (stock solution with 10 mg/mL in DMSO) were added with 1:1 protein-to-fluorophore molar ratio and incubated for 1 h at room temperature. The fluorophores and other small molecules were removed from the proteins by passing the reaction mixture through a HiTrap desalting column with buffer containing 50 mM Tris, pH 8.0, 300 mM NaCl and 1 mM TCEP.

Fluorescence labeling efficiency was measured by Nanodrop 2000 (ThermoFisher). In imaging assays, fluorescence-labeled proteins were further diluted with the corresponding unlabeled proteins in the same buffer. Dilution ratio was specified in the legend of each figure.

Imaging-based assay of phase separation

Imaging-based phase separation assays followed our previously described procedures.^{31,32} Briefly, proteins (with affinity tags cleaved and removed) were prepared in a buffer containing 50 mM Tris, pH 8.0, 100 mM NaCl, 1 mM EDTA, and 2 mM DTT and pre-cleared via high-speed centrifugations. Proteins were then mixed or diluted with buffer to designated combinations and concentrations. For imaging assay, protein samples were injected into a homemade flow chamber for DIC and fluorescent imaging with a Nikon Ni-U upright fluorescence microscope (40× lenses) or with a Zeiss LSM880 confocal microscope (63× lenses) imaging at room temperature. Images and fluorescence intensities of signals were analyzed by the ImageJ software.

ITC assay

ITC measurements were carried out on a MicroCal VP-ITC calorimeter at 25 °C. Proteins used for ITC measurements were dissolved in an assay buffer composed of 50 mM Tris, pH 8.0, 100 mM NaCl, 1 mM EDTA, and 2 mM DTT. Affinity tags on proteins were cleaved and removed. High concentration of protein was loaded into the syringe and titrated into the cell containing low concentration of corresponding interactors (concentrations for each reaction are indicated in the figure legends). For each titration point, a 10 μL aliquot of a protein sample in the syringe was injected into the interacting protein in the cell at a time interval of 2 min. Titration data were analyzed using the Origin7.0 software and fitted with the one-site binding model.

Lipid bilayer preparation and phase separation assay

Small unilamellar vesicle (SUV) preparation, cover glass washing and lipid coating, lipid bilayer phase separation assay followed our previously described procedures.³¹ Supported membrane bilayers were made of 97.9% POPC, 2% DGS-NTA-Ni²⁺ and 0.1% PE-PEG5000. 0.5 μM His₆-TARP_CT was added and incubated with SLBs for 1 h at room temperature, followed by washing with the cluster buffer (50 mM Tris, pH 8.2, 100 mM NaCl, 1 mM TCEP, 1 mg/mL BSA) for three times to remove unbound TARP_CT. Other PSD components (each in 1 μM) were added to the SLB-containing chamber to induce phase separation to occur on the lipid bilayers. Arc at the indicated concentrations were then added to assay Arc-induced TARP_CT dispersion by confocal microscopic imaging after 10 min incubation of the PSD proteins with the TARP_CT-anchored SLBs.

NMR spectroscopy

NMR samples contained 0.1 mM of the uniformly ¹⁵N-labeled GAG or GAG N-lobe in 50 mM Tris, 100 mM NaCl, 1 mM DTT and 1 mM EDTA at pH 7.0. NMR spectra were acquired at 25 °C on a Varian Inova 800 MHz spectrometer equipped with an actively z-gradient shielded triple resonance probe. The backbone assignments of Arc GAG were obtained by using the data from a previous study.³⁸

Primary hippocampal neuron culture

For synaptic dispersion of GFP-Stargazin by full-length Arc, hippocampal neurons from embryonic day 18 (E18) rats were seeded on poly-L-lysine coated coverslips. The cells were plated in neurobasal media (GIBCO) containing 50 U/mL penicillin, 50 mg/mL streptomycin, and 2 mM GlutaMax supplemented with 2% (vol/vol) B27 (GIBCO) and 5% horse serum (Hyclone). At DIV6, cells were maintained in gli-conditioned NM1 (neurobasal media with 2 mM GlutaMax, 1% FBS, 2% B27, 1× FDU, 5 mM uridine [SIGMA F0503], and 5 mM 5-Fluoro-2'-deoxyuridine [SIGMA U3003]). Cells were transfected at DIV15–18 with LipofectAMINE2000 (Invitrogen) in accordance with the manufacturer's manual. After 6–7 days, cells were fixed with 4% (vol/vol) paraformaldehyde (PFA) together with 4% (wt/vol) sucrose in 1× PBS (pH 7.5) and then mounted on slides for imaging.

For synaptic dispersion of GFP-PDFR-Stg_CT by Arc GAG, hippocampal neuronal cultures were prepared from E17 C57BL/6 WT mice hippocampi. Cells were seeded on PDL/Laminin double-coated glass coverslips (Neuvitro) in 12-well plates. The cells were plated in neurobasal media containing 50 U/mL penicillin, 50 mg/mL streptomycin, and 2 mM GlutaMax supplemented with 2% (vol/vol) B27 (GIBCO) and 10% FBS. At DIV8, cells were maintained in neurobasal media with 2 mM GlutaMax, 2% B27, 1% FBS, 1× FDU. Cells were cotransfected at DIV19 with plasmids by using Lipofectamine 2000 reagent (Invitrogen). Cells were fixed at DIV20 with 4% (vol/vol) PFA together with 4% (wt/vol) sucrose in 1× PBS (pH 7.5) and then mounted on slides for imaging.

AUC analysis

Sedimentation velocity experiments were performed on a Beckman XL-I analytical ultracentrifuge equipped with an eight-cell rotor at the speed of 32,000 rpm at 25 °C. The scans were taken for 360 times with intervals of 5 min at absorption at 280 nm. All data were calibrated with the buffer as the background. The partial specific volume of protein samples and the buffer density were calculated using the program SEDNTERP. The final sedimentation velocity data were analyzed and fitted to a continuous sedimentation coefficient distribution model using the program SEDFIT.

Quantification and statistical analysis

Statistical parameters including the definitions and exact values of n (e.g., number of experiments, number of spines, number of cells etc), distributions and deviations are reported in the figures and corresponding figure legends. Data of in vitro phase transition imaging assay were expressed as means \pm SD. Data of primary rat neuron culture were expressed as means \pm SEM and data of mouse neuron culture were expressed as means \pm SD; ns, not significant; * $P < 0.05$, ** $P < 0.01$ and *** $P < 0.001$ using one-way ANOVA with Tukey's multiple comparison test.

Data are judged to be statistically significant when $P < 0.05$ by one-way ANOVA with Tukey's multiple comparison test. None of the data were removed from our statistical analysis as outliers. Statistical analysis was performed in GraphPad Prism. All experiments related to cell cultures and imaging studies were performed in blinded fashion.

REFERENCES

- Lyford, G. L. et al. Arc, a growth factor and activity-regulated gene, encodes a novel cytoskeleton-associated protein that is enriched in neuronal dendrites. *Neuron* **14**, 433–445 (1995).
- Moga, D. E. et al. Activity-regulated cytoskeletal-associated protein is localized to recently activated excitatory synapses. *Neuroscience* **125**, 7–11 (2004).
- Steward, O., Wallace, C. S., Lyford, G. L. & Worley, P. F. Synaptic activation causes the mRNA for the IEG Arc to localize selectively near activated postsynaptic sites on dendrites. *Neuron* **21**, 741–751 (1998).
- Steward, O. & Worley, P. F. Selective targeting of newly synthesized Arc mRNA to active synapses requires NMDA receptor activation. *Neuron* **30**, 227–240 (2001).
- Link, W. et al. Somatodendritic expression of an immediate early gene is regulated by synaptic activity. *Proc. Natl. Acad. Sci. USA* **92**, 5734–5738 (1995).

- Waung, M. W., Pfeiffer, B. E., Nosyreva, E. D., Ronesi, J. A. & Huber, K. M. Rapid translation of Arc/Arg3.1 selectively mediates mGluR-dependent LTD through persistent increases in AMPAR endocytosis rate. *Neuron* **59**, 84–97 (2008).
- Maier, B., Medrano, S., Sleight, S. B., Visconti, P. E. & Scrabble, H. Developmental association of the synaptic activity-regulated protein arc with the mouse acrosomal organelle and the sperm tail. *Biol. Reprod.* **68**, 67–76 (2003).
- Vazdarjanova, A. et al. Spatial exploration induces ARC, a plasticity-related immediate-early gene, only in calcium/calmodulin-dependent protein kinase II-positive principal excitatory and inhibitory neurons of the rat forebrain. *J. Comp. Neurol.* **498**, 317–329 (2006).
- Okuno, H. et al. Inverse synaptic tagging of inactive synapses via dynamic interaction of Arc/Arg3.1 with CaMKII β . *Cell* **149**, 886–898 (2012).
- Steward, O., Farris, S., Pirbhoy, P. S., Darnell, J. & Driesche, S. J. Localization and local translation of Arc/Arg3.1 mRNA at synapses: some observations and paradoxes. *Front. Mol. Neurosci.* **7**, 101 (2014).
- Dynes, J. L. & Steward, O. Arc mRNA docks precisely at the base of individual dendritic spines indicating the existence of a specialized microdomain for synapse-specific mRNA translation. *J. Comp. Neurol.* **520**, 3105–3119 (2012).
- Rao, V. R. et al. AMPA receptors regulate transcription of the plasticity-related immediate-early gene Arc. *Nat. Neurosci.* **9**, 887–895 (2006).
- Giorgi, C. et al. The EJC factor eIF4AIII modulates synaptic strength and neuronal protein expression. *Cell* **130**, 179–191 (2007).
- Greer, P. L. et al. The Angelman Syndrome protein Ube3A regulates synapse development by ubiquitinating arc. *Cell* **140**, 704–716 (2010).
- Chowdhury, S. et al. Arc/Arg3.1 interacts with the endocytic machinery to regulate AMPA receptor trafficking. *Neuron* **52**, 445–459 (2006).
- Rial Verde, E. M., Lee-Osbourne, J., Worley, P. F., Malinow, R. & Cline, H. T. Increased expression of the immediate-early gene arc/arg3.1 reduces AMPA receptor-mediated synaptic transmission. *Neuron* **52**, 461–474 (2006).
- Shepherd, J. D. et al. Arc/Arg3.1 mediates homeostatic synaptic scaling of AMPA receptors. *Neuron* **52**, 475–484 (2006).
- Beique, J. C., Na, Y., Kuhl, D., Worley, P. F. & Huganir, R. L. Arc-dependent synapse-specific homeostatic plasticity. *Proc. Natl. Acad. Sci. USA* **108**, 816–821 (2011).
- Guzowski, J. F. et al. Inhibition of activity-dependent arc protein expression in the rat hippocampus impairs the maintenance of long-term potentiation and the consolidation of long-term memory. *J. Neurosci.* **20**, 3993–4001 (2000).
- Park, S. et al. Elongation factor 2 and fragile X mental retardation protein control the dynamic translation of Arc/Arg3.1 essential for mGluR-LTD. *Neuron* **59**, 70–83 (2008).
- Plath, N. et al. Arc/Arg3.1 is essential for the consolidation of synaptic plasticity and memories. *Neuron* **52**, 437–444 (2006).
- Wall, M. J. et al. The temporal dynamics of Arc expression regulate cognitive flexibility. *Neuron* **98**, 1124–1132 (2018).
- Manago, F. et al. Genetic disruption of Arc/Arg3.1 in mice causes alterations in dopamine and neurobehavioral phenotypes related to schizophrenia. *Cell Rep.* **16**, 2116–2128 (2016).
- Wu, J. et al. Arc/Arg3.1 regulates an endosomal pathway essential for activity-dependent beta-amyloid generation. *Cell* **147**, 615–628 (2011).
- Peebles, C. L. et al. Arc regulates spine morphology and maintains network stability in vivo. *Proc. Natl. Acad. Sci. USA* **107**, 18173–18178 (2010).
- El-Boustani, S. et al. Locally coordinated synaptic plasticity of visual cortex neurons in vivo. *Science* **360**, 1349–1354 (2018).
- DaSilva L. L. et al. Activity-Regulated Cytoskeleton-Associated Protein Controls AMPAR Endocytosis through a Direct Interaction with Clathrin-Adaptor Protein 2. *eNeuro* **3**, 0144–15 (2016).
- Blanpied, T. A., Scott, D. B. & Ehlers, M. D. Dynamics and regulation of clathrin coats at specialized endocytic zones of dendrites and spines. *Neuron* **36**, 435–449 (2002).
- Racz, B., Blanpied, T. A., Ehlers, M. D. & Weinberg, R. J. Lateral organization of endocytic machinery in dendritic spines. *Nat. Neurosci.* **7**, 917–918 (2004).
- Zhang, W. et al. Structural basis of arc binding to synaptic proteins: implications for cognitive disease. *Neuron* **86**, 490–500 (2015).
- Zeng, M. et al. Reconstituted postsynaptic density as a molecular platform for understanding synapse formation and plasticity. *Cell* **174**, 1172–1187 (2018).
- Zeng, M. et al. Phase separation-mediated TARP/MAGUK complex condensation and AMPA receptor synaptic transmission. *Neuron* **104**, 529–543 (2019).
- Zeng, M. et al. Phase transition in postsynaptic densities underlies formation of synaptic complexes and synaptic plasticity. *Cell* **166**, 1163–1175 (2016).
- Chen, X., Wu, X., Wu, H. & Zhang, M. Phase separation at the synapse. *Nat. Neurosci.* **23**, 301–310 (2020).
- Diering, G. H. et al. Homer1a drives homeostatic scaling-down of excitatory synapses during sleep. *Science* **355**, 511–515 (2017).
- Feng, Z., Wu, X. & Zhang, M. Presynaptic bouton compartmentalization and postsynaptic density-mediated glutamate receptor clustering via phase separation. *Neuropharmacology* **193**, 108622 (2021).

37. Hosokawa, T. et al. CaMKII activation persistently segregates postsynaptic proteins via liquid phase separation. *Nat. Neurosci.* **24**, 777–785 (2021).
38. Nielsen, L. D., Pedersen, C. P., Erlendsson, S. & Teilmann, K. The capsid domain of Arc changes its oligomerization propensity through direct interaction with the NMDA receptor. *Structure* **27**, 1071–1081 (2019).
39. Opazo, P. et al. CaMKII triggers the diffusional trapping of surface AMPARs through phosphorylation of stargazin. *Neuron* **67**, 239–252 (2010).
40. Park, J. et al. CaMKII phosphorylation of TARPgamma-8 is a mediator of LTP and learning and memory. *Neuron* **92**, 75–83 (2016).
41. Sumioka, A., Yan, D. & Tomita, S. TARP phosphorylation regulates synaptic AMPA receptors through lipid bilayers. *Neuron* **66**, 755–767 (2010).
42. Tomita, S., Stein, V., Stocker, T. J., Nicoll, R. A. & Brecht, D. S. Bidirectional synaptic plasticity regulated by phosphorylation of stargazin-like TARPs. *Neuron* **45**, 269–277 (2005).
43. Hafner, A. S. et al. Lengthening of the Stargazin Cytoplasmic Tail Increases Synaptic Transmission by Promoting Interaction to Deeper Domains of PSD-95. *Neuron* **86**, 475–489 (2015).
44. Inamura, M. et al. Differential localization and regulation of stargazin-like protein, gamma-8 and stargazin in the plasma membrane of hippocampal and cortical neurons. *Neurosci. Res.* **55**, 45–53 (2006).
45. Tomita, S. et al. Functional studies and distribution define a family of transmembrane AMPA receptor regulatory proteins. *J. Cell Biol.* **161**, 805–816 (2003).
46. Fukaya, M., Yamazaki, M., Sakimura, K. & Watanabe, M. Spatial diversity in gene expression for VDCCgamma subunit family in developing and adult mouse brains. *Neurosci. Res.* **53**, 376–383 (2005).
47. Guzowski, J. F., McNaughton, B. L., Barnes, C. A. & Worley, P. F. Environment-specific expression of the immediate-early gene Arc in hippocampal neuronal ensembles. *Nat. Neurosci.* **2**, 1120–1124 (1999).
48. Wallace, C. S., Lyford, G. L., Worley, P. F. & Steward, O. Differential intracellular sorting of immediate early gene mRNAs depends on signals in the mRNA sequence. *J. Neurosci.* **18**, 26–35 (1998).
49. Cheng, D. et al. Relative and absolute quantification of postsynaptic density proteome isolated from rat forebrain and cerebellum. *Mol. Cell Proteom.* **5**, 1158–1170 (2006).
50. Li, T. P., Song, Y., MacGillivray, H. D., Blanpied, T. A. & Raghavachari, S. Protein crowding within the postsynaptic density can impede the escape of membrane proteins. *J. Neurosci.* **36**, 4276–4295 (2016).
51. Berry, K. P. & Nedivi, E. Spine dynamics: are they all the same? *Neuron* **96**, 43–55 (2017).
52. Shin, S. M. et al. GKAP orchestrates activity-dependent postsynaptic protein remodeling and homeostatic scaling. *Nat. Neurosci.* **15**, 1655–1666 (2012).
53. Zhu, J. et al. Synaptic targeting and function of SAPAPs mediated by phosphorylation-dependent binding to PSD-95 MAGUKs. *Cell Rep.* **21**, 3781–3793 (2017).
54. Cai, Q. et al. CaMKIIalpha-driven, phosphatase-checked postsynaptic plasticity via phase separation. *Cell Res.* **31**, 37–51 (2021).
55. Ashley, J. et al. Retrovirus-like Gag protein Arc1 binds RNA and traffics across synaptic boutons. *Cell* **172**, 262–274 (2018).
56. Pastuzyn, E. D. et al. The neuronal gene Arc encodes a repurposed retrotransposon Gag protein that mediates intercellular RNA transfer. *Cell* **173**, 275 (2018).
57. Erlendsson, S. et al. Structures of virus-like capsids formed by the Drosophila neuronal Arc proteins. *Nat. Neurosci.* **23**, 172–175 (2020).

ACKNOWLEDGEMENTS

This work was supported by a grant from the Minister of Science and Technology of China (2019YFA0508402), a grant from the National Science Foundation of China (82188101), grants from Research Grant Council of Hong Kong (AoE-M09-12, 16104518 and 16101419), a HFSP Research Grant (RGP0020/2019) to M.Z. and a grant from National Institute of Health (RO1 NS036715) to R.H.

AUTHOR CONTRIBUTIONS

X.C., B.J., Y.A., B.L., and F.Y. performed experiments; X.C., B.J., Y.A., B.L., F.Y., R.H., and M.Z. analyzed data; X.C., B.J., Y.A., M.Z. designed the research; X.C., B.J., M.Z. drafted, all authors commented on the paper; M.Z. coordinated the project.

COMPETING INTERESTS

The authors declare no competing interests.

ADDITIONAL INFORMATION

Supplementary information The online version contains supplementary material available at <https://doi.org/10.1038/s41422-022-00697-9>.

Correspondence and requests for materials should be addressed to Mingjie Zhang.

Reprints and permission information is available at <http://www.nature.com/reprints>